

## FINITE ELEMENT ANALYSIS OF RC BEAM STRENGTHENED WITH PCM

Mahmudul H. MIZAN\*<sup>1</sup>, Tamon UEDA\*<sup>2</sup>, Jun TAKAHASHI\*<sup>3</sup>

## ABSTRACT

Polymer Cement Mortar (PCM) overlaid to the tension side surface of reinforced concrete RC structure often performs to upgrade the flexural capacity and stiffness. PCM strengthened RC structure may fail in premature debonding before yielding of rebar or upper concrete crushing. This study aims in developing a two-dimensional finite element numerical analysis in DIANA. Comparisons between analytical and experimental results confirm that this numerical approach is appropriate for estimating the load-carrying capacity and failure behavior of RC beams strengthened with PCM layer.

**Keywords:** Polymer cement mortar, load carrying capacity, failure modes, numerical model.

## 1. INTRODUCTION

In the last several decades, various strengthening techniques like external post-tensioning, steel plate, continuous fiber sheet, and polymer cement mortar (PCM) are developed that is bonded to the tension side surface of existing reinforced concrete RC member to increase the flexural load carrying capacity and stiffness. In PCM retrofitting methods, the strengthening bars are fixed underneath the RC members and then covered with sprayed/troweled PCM. Though PCM is known as good repair material due to its higher bond strength and lower permeability, the interface between substrate concrete and PCM is considered the weakest link in the structure and are susceptible to brittle debonding failures [1]. Experimental observation [2] has shown different debonding failure modes of PCM overlay. To date, different debonding failure modes like concrete cover separation, peeling off in the constant moment zone, peeling off in the shear flexure and overlay end zone are reported [3]. In PCM strengthened RC beam, debonding failure either initiates owing to flexure or shear crack or at the edge of the overlay due to stress concentration [4]. Premature failure modes are also reported in case of FRP sheet and steel plate like PCM strengthening [5,6].

Finite element analysis is one of the approaches to estimate the load-carrying capacity of the beam failed by this debonding mode. To numerically simulate the load-carrying capacity of the PCM repaired beam, the study [7] used Mohr-Coulomb interface model to consider the interaction between concrete and PCM with normal and shear stiffness as  $1000 \text{ N/mm}^3$ . Different interface behavior was also reported by different author in simulating the RC beam strengthening with FRP, steel plate etc. A typical bond-slip relationship as shown in Fig. 1 is presented [8]. Along with Popovic's equation [9], this type of interface behavior can also be used in simulating PCM strengthening RC beam.

In this paper, bilinear bond-slip is used at the

concrete-PCM interface. The important parameters in defining this interface behavior are interface bond strength,  $\tau_{imax}$  and interface fracture energy,  $G_i$  that depends predominately on the properties of substrate concrete as reported by the experimental observation based on interface shear test on pure shear specimen [10].

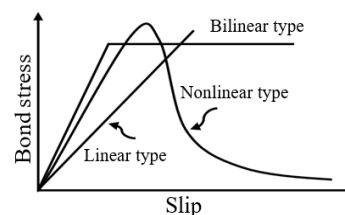


Fig. 1 Typical interface bond-slip relationship

A two-dimensional finite element analysis by DIANA is used in this paper to simulate the load-carrying capacity and failure modes of RC beams strengthened with PCM. In this method, the smeared rotating crack approach is employed to show the crack behavior, along with fib interface model of the axial rebar and bilinear bond-slip relationship at PCM-concrete interface. The analysis results are compared with the experimental results obtained from four-point bending test conducted by the past studies [2,11] for the applicability of the proposed numerical model. However, bond stress distribution along the interface is not focused this time and it will be considered in our further study.

## EXPERIMENTAL OVERVIEW

In this study, strengthening RC specimens with varying shear span ratio between 4 to 8 and cross-section as  $200\text{mm} \times 150\text{mm}$  is used to confirm the applicability of the proposed numerical analysis method. Stirrups were placed at an interval of 75 mm and PCM were bonded having a thickness of 30 mm to the tension side

\*1 Master's student, Lab. of Engineering for Maintenance System, Hokkaido University, JCI Student Member

\*2 Professor, Lab. of Engineering for Maintenance System, Hokkaido University, JCI Fellow Member

\*3 Denka Co., Ltd., Chuo-ku, Tokyo, Japan, JCI Member

Table 1: Properties of concrete and PCM of the PCM overlaid RC beam

Beam	$a$ (mm)	$f'_c$ (MPa)	$f_{ct}$ (MPa)	$E_{con}$ (MPa)	$f'_{o}$ (MPa)	$f_{ot}$ (MPa)	$E_o$ (MPa)	$t$ (mm)	$d_r$ (mm)	$d_{rc}$ (mm)	$d_s$ (mm)
SK4-2-S2(3)	460	38	2.7	33700	27.6	2.89	12100	30	115	30	155
SK6-2-S2(3)	690	38	2.7	33700	27.6	2.89	12100	30	115	30	155
SK8-2-S2(3)	920	38	2.7	33700	27.6	2.89	12100	30	115	30	155
DZ4-2-S2(3)	460	59.4	3.5	33000	57.4	3.8	23400	30	116	31	170

of the RC beam leaving 50 mm gap between the overlay and supporting end. The tabulated values of the material properties of concrete and steel in Table 1 and Table 2 are the same values as in references [2,11] which were obtained from the experimental test results.

The acronym designation adopted for beams shown in Table 1 are as follows: the first letter is the word character SK and DZ designating for author name; the first number appearing after author name represents shear span ratio; the following number indicates number of tension and compression reinforcement bars in the concrete part (10 mm diameter bar); the letter S designating for strengthening bar (10 mm diameter bar) while the last number (2 and 3) represents the number of strengthening bar and distinguishes two beams in same series. Table 1 also shows the material properties of concrete and PCM, where  $a$ ,  $t$ ,  $d_{rc}$ ,  $d_r$ , and  $d_s$  denote shear span ratio, thickness of the PCM overlay, distance from beam compression face to the centroid of steel compression reinforcement, distance from beam compression face to the centroid of steel tension reinforcement, distance from beam compression face to the centroid of strengthening reinforcement, and  $f'_{c(o)}$  is the cylinder compressive strength,  $f_{c(o)t}$  is the tensile strength, and  $E_{con(o)}$  is the modulus of elasticity of concrete and overlay material (PCM), respectively.

Table 2 shows the properties of reinforcement in concrete and overlay section where  $E_{r(c,t,v,s)}$  denotes the modulus of elasticity,  $f_{y(c,t,v,s)}$  is the yield strength,  $f_{u(c,t,v,s)}$  is the ultimate strength of the compression, tension, shear and strengthening reinforcement.

Table 2: Characteristics of reinforcement

Beam	$E_{r(c,t,v,s)}$ (MPa)	$f_{y(c,t,v,s)}$ (MPa)	$f_{u(c,t,v,s)}$ (MPa)
SK beams	188000	386	532
DZ beams	190000	357	520

### 3. FINITE ELEMENT ANALYSIS

The numerical analysis has been performed with a plane stress finite element model in DIANA 10.1 [12], the schematic diagram of the FEM element of half beam considered for the analysis is shown in Fig. 2. For this numerical modeling, the steel reinforcement is modeled as bar type element which is embedded in the concrete. The half beam is considered due to symmetry of the beam and it will reduce the simulation time. All the nodes along the center line are fixed only in the horizontal direction, while one node at the bottom of support plate is fixed only in the vertical direction. The load is applied

as prescribed displacement at one node of the top of loading plate.

The loading and support plates of steel with assumed dimension 60x20 mm is introduced and modeled using eight nodes quadrilateral elements to limit the stress concentration occurring in the concrete elements around the loading and supporting points. An incremental monotonic displacement is applied in simulating the test conditions.

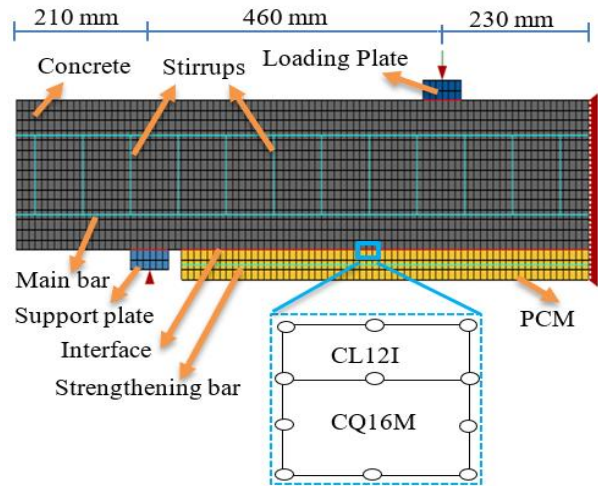


Fig. 2 Schematic diagram of half RC beam (DZ series) as an example) with the boundary condition

In the numerical procedure, displacement control incremental iterative solution procedure is adopted. The displacement and force convergence rules along with line-search procedure specified in DIANA were employed based on Quasi-Newton (secant) method.

#### 3.1 Modeling of material

The CQ16M i.e. eight nodes quadrilateral isoperimetric with nine-point (Gaussian) numerical integration plane stress element as shown in Fig. 2 is used to build the material model for concrete and PCM. The total strain based rotating crack model with a thickness of 200 mm is considered for cracking in concrete and PCM.

A non-linear tension stiffening proposed by Hordijk [13] as shown in Fig. 3(a) and Thorenfeldt parabolic curve [14] as shown in Fig. 3(b) was applied to the stress-strain relationship of concrete and PCM in tension and compressive area respectively. The input parameters, modulus of elasticity, tensile and compressive strength for this model can be drawn from Table 1 and the tensile and compression fracture energy is calculated with the assumption formula from JSCE

Standard Specifications [15] and proposed formula [16] as shown in Eqs. 1 and 2 respectively where  $d_{max}$  is the maximum aggregate size (mm) and  $f'_c$  is the compressive strength of concrete (MPa).

$$\text{Tensile Fracture Energy, } G_t = \frac{\sqrt[3]{d_{max} \cdot f'_c}}{100} \quad (1)$$

$$\text{Compressive Fracture Energy, } G_f = 8.8 \cdot \sqrt{f'_c} \quad (2)$$

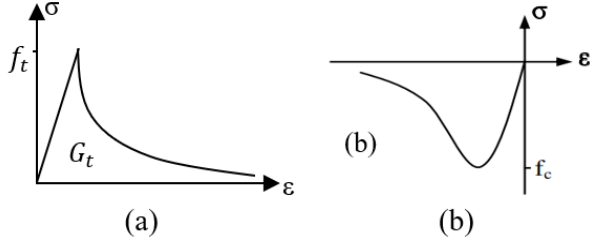


Fig. 3 Constitutive model of Concrete and PCM (a) tension, (b) compression

The reinforcements are defined as an ideal plasticity material with the yield condition of Von Mises as shown in Fig. 4(a). The stirrups are modeled as embedded reinforcement considering perfect bond between stirrup and concrete and for the main rebar, the bond-slip relationship is considered based on the curve shown in Fig. 4(b) by fib model code 2010 [17]. Steel plates are modeled as elastic isotropic material with a modulus of elasticity and poisson ratio as 210GPa and 0.3 respectively.

For the interface between concrete and PCM, the element is modeled using CL12I. The CL12I element is interfaced element between two lines in a two-dimensional configuration with six nodes and zero thickness. This numerical model used a bilinear bond-slip relation as shown in Fig. 4(c) to simulate the interface behavior of concrete and PCM.

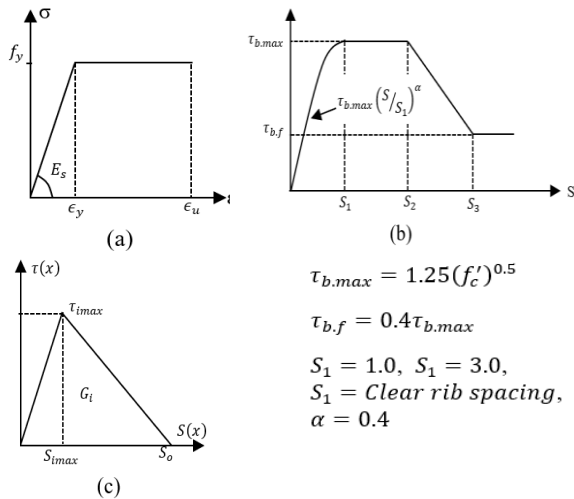


Fig. 4 Material models (a) stress-strain relationship of the rebar, (b) stress-relative displacement relationship for the interface between concrete and rebar, (c) stress-relative displacement relationship for the interface between concrete and PCM.

The material properties for the interface model between concrete and PCM, interface bond strength and

interface fracture energy, are calculated based on Eqs. 3 and 4 respectively [18], where  $f'_c$  and  $f_t$  is the compressive and tensile strength of concrete respectively. The coefficients,  $C_{\tau i}$  and  $C_{G i}$  of the equations are assumed to be 0.711 and 0.075 as observed from the experiment [19].

$$\tau_{imax} = C_{\tau i} \left( \frac{1}{f'_c} + \frac{1}{f_t} \right)^{-1} \quad (3)$$

$$G_i = C_{G i} \cdot f'_c{}^{1/3} \quad (4)$$

## 4. RESULTS AND DISCUSSIONS

### 4.1 Load and displacement

The simulated beam is verified by the experimental result based on the load-displacement curve. In fig. 5, it shows the relationship between total load and mid-span displacement of the experimental and FE analysis results of two beams of DZ series with different strengthening bar amount. It seems that in the simulation the amount of reinforcement in PCM does not affect the initial stiffness although some changes is observed in the experimental curve. The load in the numerical analysis is decreasing at one stage due to discontinuity by some major cracks occur in concrete and after that the load increases again because tensile steel did not reach its yield strength at that stage and it carries load transferred from the major cracks. Sudden drop of the load value corresponds to the structural failure of the beam by debonding while plateaued load-displacement relation indicates flexural failure mode. The increase of overlay reinforcement amount increases the ultimate load but premature debonding failure mode observed in the beam with higher overlay reinforcement both in experimental and numerical curves. The results are reasonable in regards of load carrying capacity and failure modes. The cracking pattern which indicates the failure mode is also presented in the later part.

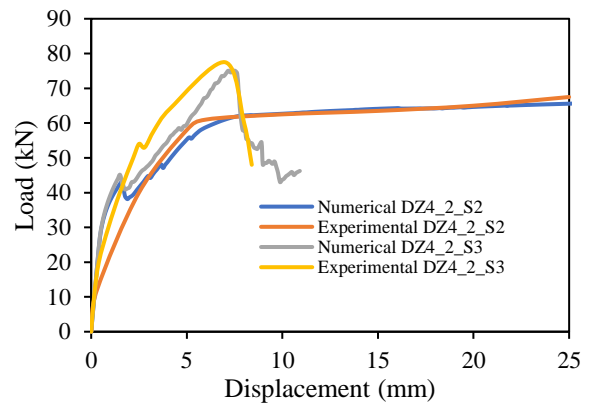


Fig. 5 Load-displacement result of both experimental and FE analysis of DZ series beam

In Fig. 6(a-c), it shows the experimental and EF analysis results of the load-displacement diagram of SK series beam with different shear span ratio. The initial stiffness and peak load of the simulation curve matches considerably with experimental curve expect for the beam SK4-2-S2 that shows 27% difference in peak load. The load-displacement relation of the beam shows a

sudden drop of the load value in case of the beam SK4-2-S2 and SK6-2-S2 while the beam SK8-2-S2 has plateaued in diagram, both in case of experimental and FE analysis results. It is thought that the beams failed with premature debonding failure with a sudden drop of the load whereas SK8-2-S2 beam does not show this behavior showing a plateau in the curve indicating a

flexural failure mode.

In Fig. 6(d), the results with different shear span ratios are compared. The ductility is increased with the increase of the shear span ratio (3 times in shear span ratio 6 and 8 times in shear span ratio 8 than in shear span ratio 4), but peak load is decreased with the increase of shear span ratio.

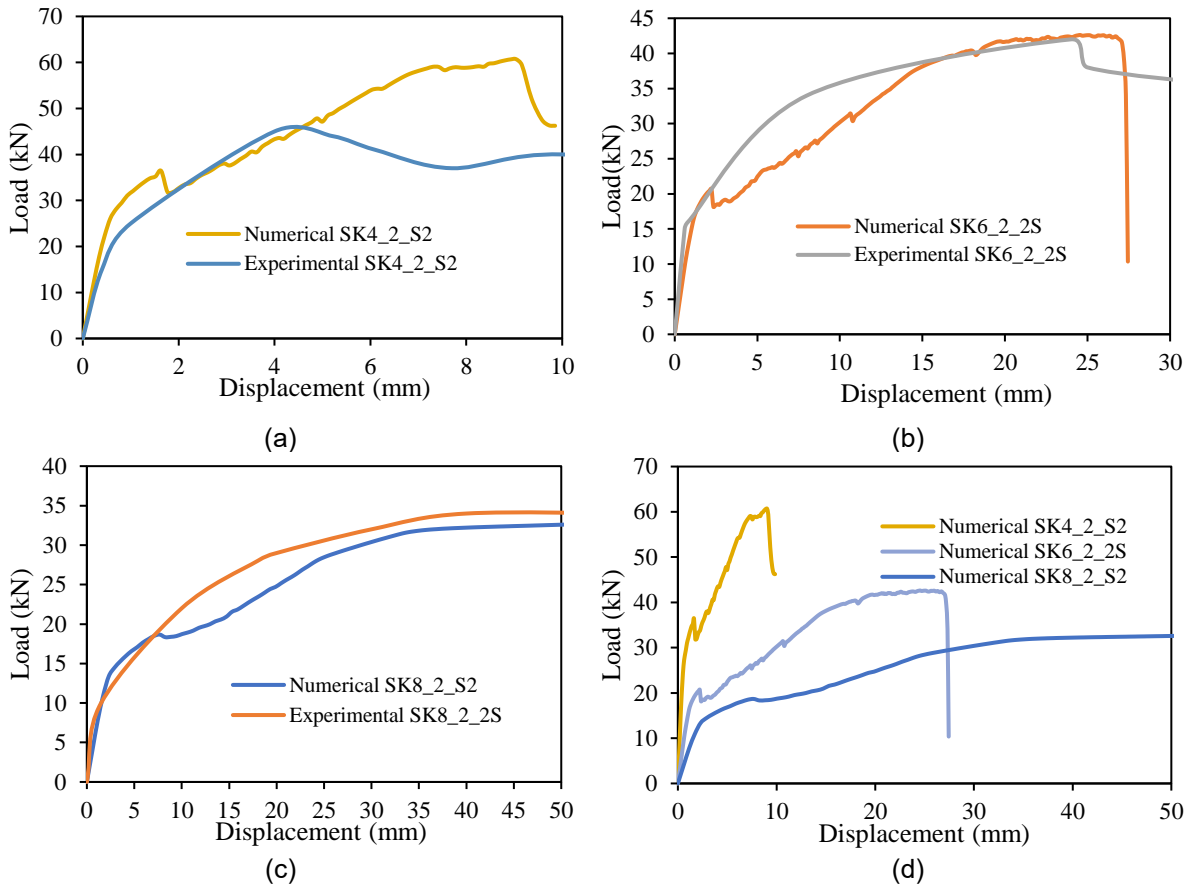


Fig. 6 Load-displacement result of experimental and FE analysis of SK series beam (a) Shear span ratio 4, (b) shear span ratio 6, (c) shear span ratio 8, and (d) comparison among different shear span ratio cases.

Table 3: Load carrying capacity and failure modes of the experimental and simulated strengthened beam

Beam	Peak Load (kN)		Failure Mode	
	(Exp.)	(Simulation)	(Exp)	(Simulation)
DZ4-2-S2	69.38	68.12	Flexural	Flexural
DZ4-2-S3	76.91	75.07	Concrete cover separation	Concrete cover separation
SK4-2-S2	54.43 43.98	60.69	Peeling in central zone Peeling in central zone	Peeling in shear flexure zone
SK4-2-S3	65.31 67.67	67.33	Peeling in overlay end zone Peeling in overlay end zone	Peeling in overlay end zone
SK6-2-S2	42.81 39.42	42.57	Peeling in central zone Peeling in central zone	Peeling in central Zone
SK6-2-S3	41.34 46.77	51.62	Peeling in central zone Peeling in shear flexure	Peeling in shear flexure zone
SK8-2-S2	32.51 31.33	34.72	Flexural Peeling in central zone	Flexural
SK8-2-S3	38.69 39.57	39.5	Flexural Peeling in central Zone	Peeling in central zone

The peak load and failure mode of all the simulated beams are tabulated in Table 3. The

comparison of experimental and numerical peak load shows good agreement except for some cases as in Fig.7.

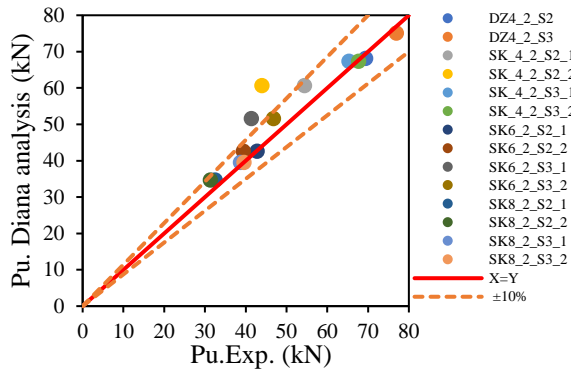


Fig. 7 Comparison of experimental and numerical peak load results.

#### 4.2 Crack patterns and failure modes

The numerical failure mode is determined with the crack formation and propagation with the increase of the load. The numerical crack pattern is also compared with the experimental crack pattern. Fig. 8 shows the numerical (half beam) and experimental (full beam) crack pattern. In Fig. 8(a), conventional crack pattern observed in the constant moment and shear flexure zone. With the increase of load, crack widen and propagate towards compression region and the beam failed due to the flexural crack. In Fig. 8(b), major crack is seen in the overlay end zone and it goes up to the main reinforcement in concrete part and propagates along the rebar. The decrease of the load with the crack propagation along rebar indicates the premature debonding failure mode known as concrete cover separation. Similar failure pattern in the experiment in the photo indicates the accuracy of the numerical simulation.

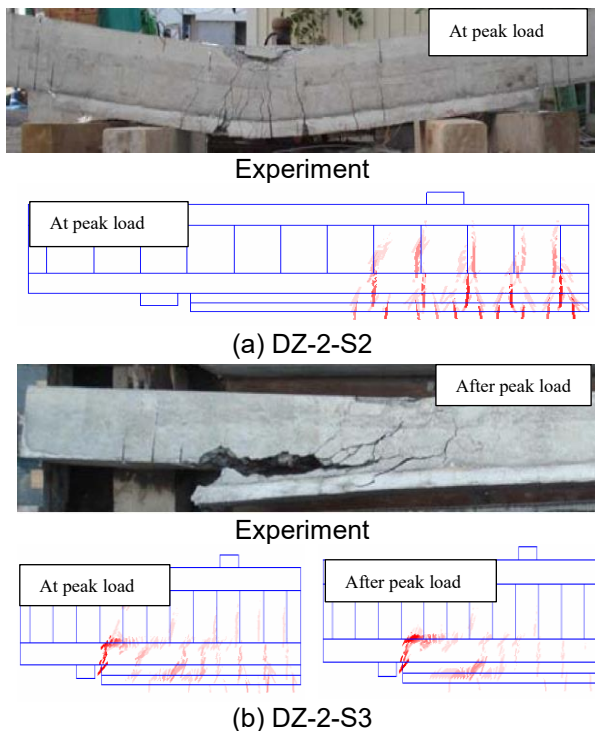


Fig. 8 Crack pattern in experiment and simulation of DZ series beam.

The numerical crack pattern of the SK series beams at peak load and after peak load level are presented in Fig. 9(a-f). In the Fig. (a-b), experimental crack patterns of the beam SK4-2-S2 and SK4-2-S3 available in the literature are also presented. It appears that at peak load level, crack start propagating along the concrete-PCM interface. The decrease of the load (illustrated in the load-deflection diagram in previous section) with the further propagation of crack along the interface indicates debonding failure mode. Similar cracking pattern in all the SK series beam indicates the debonding failure modes except the beam SK8-2-S2 that have flexural cracking pattern as shown in Fig. 9(f).

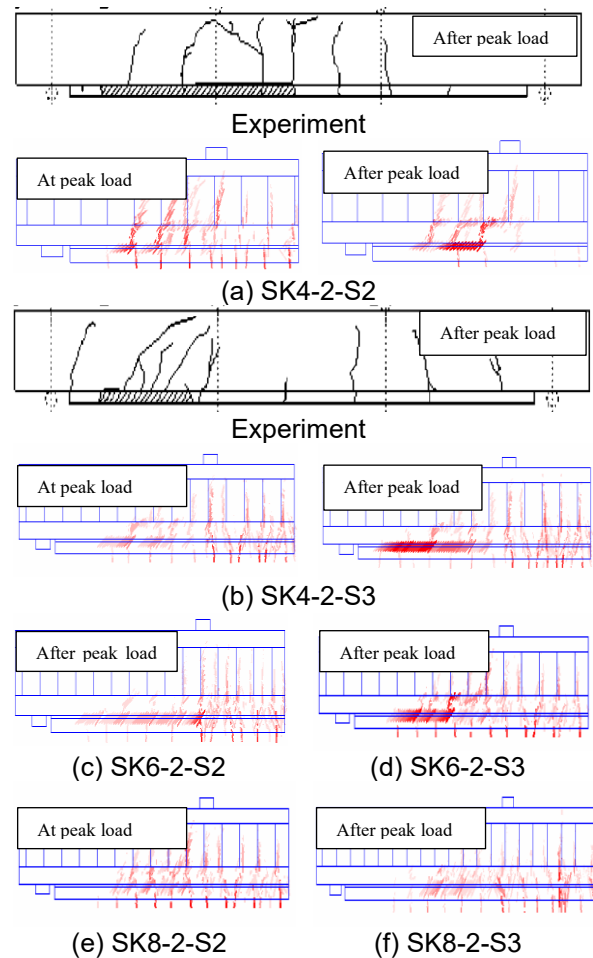


Fig. 9 Numerical crack pattern of SK series of beam.

The debonding crack is initiated at different position of the beam and propagated along the interface in either ends. According to the position of crack initiation and propagation along the beam, the failure mode of the beams are identified as peeling off in the central zone for the beam SK6-2-S2 and SK8-2-S3, peeling off in shear flexure zone for SK4-2-S2 and SK6-2-S3, peeling off in the overlay end zone for SK4-2-S3, and flexural failure for SK8-2-S2. The failure mode of all the simulated beam is tabulated in Table 2 and compared with the experimental failure mode of the beam.

## CONCLUSIONS

The following conclusions are obtained from the finite element analysis:

- Peak load is increased with the increase of the strengthening bar amount in PCM strengthening beam as experimental results.
- The debonding failure mode becomes dominant with the increase of the strengthening bar as experimental results.
- Ductility of the beam increases significantly with the increase of shear span ratio but the peak load of the beam reduced.
- Bilinear bond-slip relationship of PCM-Concrete interface can predict the experimental load carrying capacity of the beam failing with debonding with an acceptable range of accuracy.
- Failure mode based on cracking pattern matches well with the experimental failure mode.

## ACKNOWLEDGMENT

The author would like to acknowledge the scholarship grant provided by the Japanese Government under Top Global University project.

## REFERENCES

- [1] K. Rashid, T. Ueda, D. Zhang, K. Miyaguchi, and H. Nakai, "Experimental and analytical investigations on the behavior of interface between concrete and polymer cement mortar under hygrothermal conditions," *Construction and Building Materials*, vol. 94, pp. 414–425, 2015.
- [2] K. Satoh and K. Kodama, "Central Peeling Failure Behavior of Polymer Cement Mortar Retrofitting of Reinforced Concrete Beams," *Journal of Materials in Civil Engineering*, vol. 17, pp. 126–136, 2005.
- [3] D. Zhang, T. Ueda, and H. Furuuchi, "Intermediate Crack Debonding of Polymer Cement Mortar Overlay-Strengthened RC Beam," *Journal of Materials in Civil Engineering*, vol. 23, pp. 857–865, 2011.
- [4] D. Zhang, T. Ueda, and H. Furuuchi, "Concrete Cover Separation Failure of Overlay-Strengthened RC beams," *Construction and Building Materials*, vol. 26, pp. 735–745, 2012.
- [5] S. T. Smith and J. G. Teng, "FRP-strengthened RC beams. II: Assessment of debonding strength models," *Engineering Structures*, vol. 24, pp. 397–417, 2002.
- [6] H. N. Garden, R. J. Quantrill, L. C. Hollaway, A. M. Thorne, and G. A. R. Parke, "Experimental study of the anchorage length of carbon fibre composite plates used to strengthen reinforced concrete beams," *Construction and Building Materials*, vol. 12, pp. 203–219, 1998.
- [7] L. M. Mauludin, "Numerical modeling reinforced concrete beams repaired with polymer modified mortar," masters thesis, University of Padova, Italy, 2009.
- [8] B. Ghiassi, G. Marcari, D. V. Oliveira, and P. B. Lourenço, "Numerical analysis of bond behavior between masonry bricks and composite materials," *Engineering Structures*, vol. 43, pp. 210–220, 2012.
- [9] R. Bahsuan, S. Hino, K. Yamaguchi, and A. Komori, "Flexural Strengthening Effect of CFRP Strand Sheets and PCM on RC Beams," *Technical Paper*, Japan Concrete Institute, vol. 37, No. 2, 2015.
- [10] T. Ueda, D. Zhang, H. Furuuchi, and A. Hori, "Bond Strength of PCM-Concrete Interfaces : Influence of Interface Roughness and Substrate Concrete," *Technical Paper*, Japan Concrete Institute, Vol. 31, No. 1, 2009.
- [11] Z. Dawei, "Research on PCM-Concrete Interface and PCM-Strengthened RC Beam," Ph.D. thesis, Hokkaido University, Japan, 2009.
- [12] DIANA 10.1, "DIANA Finite Element Analysis User's Manual" Deflt, Netherlands.
- [13] D. A. Hordijk, "Local Approach to Fatigue Concrete," 1991.
- [14] E. Thorenfeldt, A. Tomaszewics, and J. Jensen, "Mechanical Properties of High-Strength Concrete and Application in Design," *Proceeding of Symposium Utilization of High-Strength Concrete*, Stavanger, Norway, 1987.
- [15] Japan Society of Civil Engineering Concrete Committee, "Standard Specifications for Concrete Structures," 2013.
- [16] T. Nakamura, H. Higai, "Compressive fracture energy and fracture zone length of concrete," Seminar on post-peak behavior of RC structures subjected to seismic loads, JCI-C51E, Vol.2, 259-272, 1999.
- [17] CEB FIP (2010). Model Code 2010: First complete draft, Volume 1, March 2010.
- [18] D. Ferreira, E. Oller, A. Marí, and J. Bairán, "Analysis of FRP Shear Strengthening Solutions for Reinforced Concrete Beams Considering Debonding Failure," *Journal of Composite Construction*, vol. 20, 2016.
- [19] K. Satoh and K. Kodama, "Study on peeling behavior of bond interface of concrete members retrofitted by surface overlaying with polymer cement mortar.," *Proc., JSCE*, vol. V-59, no. 732, pp. 77–87, 2003.